Title

Signatures of wakefield acceleration in astrophysical jets via gamma-rays and UHECRs

Journal

Monthly Notices of the Royal Astronomical Society, 522(4)

ISSN

0035-8711

Authors

Huxtable, Gregory B

Eltawil, Noor

Feng, Wei-Xiang

et al.

Publication Date

2023-05-11

DOI

10.1093/mnras/stad1303

Monthly Notices of the ROYAL ASTRONOMICAL SOCIETY

MNRAS **522,** 5402–5414 (2023) https://doi.org/10.1093/mnras/stad1303
Advance Access publication 2023 May 8

Signatures of wakefield acceleration in astrophysical jets via gamma-rays and UHECRs

Gregory B. Huxtable,[1]★ Noor Eltawil,[1] Wei-Xiang Feng,[2] Gabriel Player,[1] Wenhao Wang,[1] Toshiki Tajima[1]★ and Toshikazu Ebisuzaki[3]

[1]*Physics and Astronomy, UC Irvine, 4129 Frederick Reines Hall, Irvine, CA 92697, USA*
[2]*Physics and Astronomy, UC Riverside, 900 University Ave., Riverside, CA 92521, USA*
[3]*Computational Astrophysics Laboratory, RIKEN, 2-1 Hirosawa, Wako, Saitama 351-0198, Japan*

Accepted 2023 March 23. Received 2023 March 22; in original form 2022 February 25

ABSTRACT

We present six case studies from a comprehensive mass range (1–10^9 $M_\odot$) of astrophysical objects, each of which possess jets, emit high-energy gamma radiation and in some instances spatially identifiable ultra-high-energy cosmic rays (UHECRs). All sources are strong candidates for UHECR emission, if not already known to emit them. We surmise that wakefield acceleration in conjunction with the magnetorotational instability of the accretion disc explains both structural properties of the jets and details in their emission signals, such as correlations in neutrino and gamma-ray bursts, and in the case of blazars, anticorrelations in flux and spectral index. Furthermore, our model predicts an upper bound for the energy of UHECRs emitted from a source given the mass of its central compact object and total jet luminosity. To provide context for our model predictions, we quantitatively compare them with observational data, however, we have not accounted for the GZK limit and assumed universal values for several model parameters (e.g. jet-spreading index, p) that likely differ between sources. Since the accretion and acceleration mechanisms are independent of mass, aside from determining maximum values, blazars ($\sim 10^9$ $M_\odot$), radio galaxies ($\sim 10^8$ $M_\odot$), Seyfert galaxies ($\sim 10^6$ $M_\odot$), starburst galaxies ($\sim 10^3$ $M_\odot$), even microquasars (1–10 $M_\odot$) interestingly exhibit the same physics. Other radiation bands, such as X-ray, ultraviolet, or radio, may harbour additional information, but we chose not to focus on them for brevity. However, such an endeavour may open the door to a new multimessenger approach for understanding these objects.

Key words: accretion, accretion discs – neutrinos – cosmic rays – galaxies: jets – quasars: general – gamma-rays: general.

1 INTRODUCTION

A wide scope of astrophysical objects ranging from blazars, radio galaxies, Seyfert galaxies, starburst galaxies, and even microquasars emit intense high-energy gamma-rays ($\geq$10 GeV), often in spatially (localized) and temporally identifiable fashions. From each respectable class we chose to study at least one object that is known to host jets – columns of accelerated plasma extending from the poles of the central compact object [either a black hole (BH) or neutron star (NS)] – as case studies to quantitatively compare their emissions with our theory. Wakefield acceleration (WFA) primarily has implications on ultra-high-energy cosmic rays (UHECRs), high-energy neutrinos, gamma-rays and X-rays, but the theory has milder implications on optical-band light and radio emissions. Most of the selected objects emissions are spatially localized. Some also exhibit temporal structure in their signals, characteristic of WFA. The emissions often are created simultaneously, such as the coincidental 'bursts' of high-energy gamma-rays and neutrinos recently detected in blazar TXS 0506+056 (IceCube Collaboration 2018b; Garrappa et al. 2019; Rodrigues et al. 2021). Inspired by spatially pinpointed, and temporal coincidences in various emission types from sources possessing jets, we decided to quantitatively compare these observational features with WFA, a mechanism that can readily give rise to such characteristics (Ebisuzaki & Tajima 2014a, b; Tajima, Yan & Ebisuzaki 2020). This endeavour has already garnered interest from the broader scientific community (Kole 2021) as a new acceleration mechanism potentially capable of shedding light on the mystery that are UHECRs in addition to coincidental gamma-ray bursts (GRBs) and neutrino events. It is argued that the compact central objects (active galactic nuclei, or active stellar binaries) can accompany accretion disc and jets (Shibata & Uchida 1986; Tajima & Shibata 1997; Chatterjee et al. 2019). Under these circumstances, in spite of the disparate central masses among the selected objects, similar physical sequences and observational features may be expected. The structure and dynamics, we study in theory and find in observations, lead to unique and characteristic spatial, temporal, and energetic features. In Sections 3–8, we show that many of the various emission signals observed agree with their corresponding predicted values from our theory. However, we have forgone providing accurate analyses of the UHECR flux we might expect to see from Earth for each particular source. This is because intergalactic magnetic fields, the angle between our line of sight (LOS) and the polar axes of the accreting object, and the power-law index, p, that determines the rate of spreading for a given source's jets all heavily factor into providing an accurate estimation of the UHECR flux we might expect to arrive

★ E-mail: huxtablg@uci.edu (GBH); ttajima@uci.edu (TT)

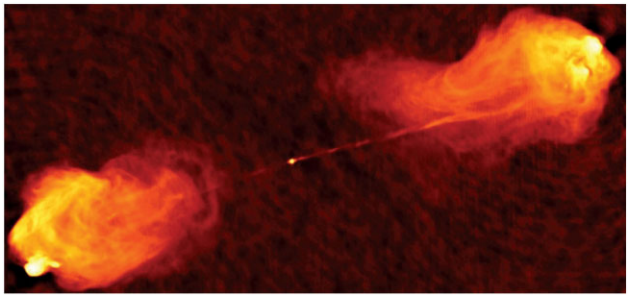

Figure 1. VLA image of the radio galaxy Cygnus A (3C 405) with its jets and giant radio lobes (credit: NRAO/AUI). Matter is accreted from the inner disc (central bright dot) orbiting the central BH and subsequently expelled, creating bipolar jets (right and left thin lines extending from the accretion disc). It is visually evident that the jets are stable (absence of plasma instabilities) for the majority of their length, until their kinetic energy has depleted substantially and begins to interact with the ambient plasma, forming turbulent gaseous lobes (top right and lower left cocoon) at the end of both jets. We consider WFA in the thin, elongated jet.

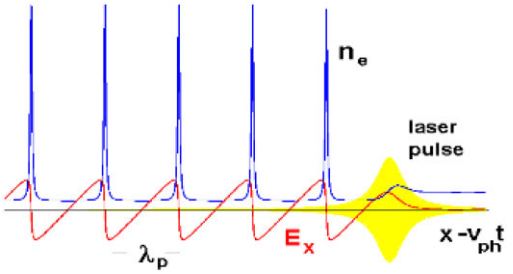

Figure 2. Classic wakefield simulation depicting the trailing electrostatic field in red, electron density in blue, and the driving laser pulse in yellow. The clear coherency due to the high phase velocity (in fact relativistic) wakefields is demonstrated (after Tajima et al. 2020).

at Earth. Instead we opted to report the total values, as if an observer were to capture all of the emitted UHECRs. Other acceleration mechanisms, such as first-order Fermi shock acceleration (Bell 1978; Blandford & Eichler 1987), magnetic reconnection (MR; de Gouveia Dal Pino & Lazarian 2005; de Gouveia Dal Pino & Kowal 2015; Rodriguez-Ramirez, de Gouveia Dal Pino & Alves Batista 2019), and turbulent heating/acceleration (O'Sullivan, Reville & Taylor 2009) are compared in contrast.

The high-energy phenomena associated with accreting BHs has been observed with gamma-ray emission. First, The Fermi Gamma-ray Space Telescope, formerly GLAST (Gamma-ray Large Area Space Telescope) launched in 2008 (Michelson, Atwood & Ritz 2010) observed accreting BHs such as active galactic nuclei (AGNs) and binary BHs in the GeV–100 GeV region (Abdo et al. 2010; Ackermann et al. 2011, 2012). In addition, air Cherenkov telescopes, such as MAGIC (Djannati-Atai 2009), H.E.S.S. (Djannati-Atai 2009), or VERITAS (Ragan 2012) and water Cherenkov detector such as High Altitude Water Cherenkov (HAWC) observatory (DeYoung 2012) observed accreting BHs in TeV and multi TeV gamma rays.

Cosmic rays vary from modest to extremely high energies (5×10^{19} eV and beyond). The conventional theory of first-order Fermi shock acceleration has been successful in explaining the universal spectral index of approximately 2 (Kotera & Olinto 2011) for UHECR energy. However, beyond 10^{19} eV, protons begin to radiate their energies in very large quantities due to synchrotron radiation if they are bent by magnetic fields (as required by Fermi acceleration) or other collisions, since the radiated energy scales quartically with the Lorentz factor of the particle (Jackson 1999). None the less, observations have detected UHECRs with energies beyond 10^{20} eV coming from localized origins (Abraham et al. 2008; He et al. 2016; di Matteo, Fujii & Kawata 2019). Wakefield accelerates particles collinear to the propagation of the wave (see Figs 1 and 2) and therefore they suffer no inherent energy loss. This also implies UHE signals generated by WFA should be emitted axially from the jets.

We now consider the likely scenario that electromagnetic pulses are produced in the jets near the innermost part of the accretion disc. When large amounts of matter suddenly accretes on to the central compact object, the magnetic field at the base of the jet is perturbed, creating an extremely intense electromagnetic wave capable of accelerating charged particles to very high energies by electromagnetic wave–particle interaction via wakefields (Tajima et al. 2020). The episodic, eruptive accretion from the disc caused by the magnetorotational instability (MRI; Balbus & Hawley 1991), hereafter referred to as MRI, can give rise to such strong electromagnetic pulses, which act as the drivers of the collective acceleration of the pondermotive force. The pondermotive force drives the electrostatic wakes that follow behind, similar to a duck or boat creating a wake behind it as it moves through the water, which trap and accelerate protons. The accelerated protons are released to the intergalactic space and some eventually reach, and decay in Earth's atmosphere as UHECRs. Some of them collide with slower protons in the jet, or the gaseous lobes to produce secondary particles, such as neutrinos and gamma-rays. The high-energy electrons, on the other hand, driven by the pondermotive force in front of the wave emit photons as a result of their orbits, and from collisions with electromagnetic perturbances, to produce various non-thermal emissions [radio, infrared (IR), visible, ultraviolet, and gamma-rays].

A charged particle can be trapped by a plasma wave (wakefield), and thus accelerated only if its velocity is within the trapping velocity width of the wave, $v_{\rm tr} = \sqrt{qE/mk}$, where E is the electrostatic field created by the plasma wake, k is the wavenumber, and q and m are the charge and mass of the particle, respectively (O'Neil 1965). Typically $v_{\rm ph} > > v_{\rm th}$ when exciting wakefields, where $v_{\rm ph}$ is the phase velocity of the wave, and $v_{\rm th}$ is the thermal velocity of the plasma. Otherwise, if $v_{\rm ph} \sim v_{\rm th}$, then the wave is resonant with the bulk plasma and instabilities such as the drift wave instability can occur and the wakefield is unstable (Tajima et al. 2020). When the wave is intense enough such that $v_{\rm tr} \sim v_{\rm ph} > > v_{\rm th}$ the wakefield traps the bulk of the plasma and is stable. We also note that in addition to the particle acceleration being collinear to the electrostatic wake, the acceleration gradient is constant in time (before the wave begins to dissipate) and Lorentz invariant, making WFA very efficient (see Fig. 1).

In a typical young star-forming galaxy with an AGN, the rotational plasma motion around the AGN amplifies the immersed magnetic field of the disc leading to large accretion events (Balbus & Hawley 1991; Matsumoto & Tajima 1995; Ebisuzaki & Tajima 2014a). This accretion is followed by the Shibata & Uchida (1986) magnetohydrodynamic (MHD) propulsion of the accretion jets with a remarkable structure formation, whose relativistic factor of the jet motion, Γ, may be as large as 10^3. Such jets can exhibit a huge spatial extent and structural integrity over 10–10^3 times the accretion disc diameter. Typically, the well collimated, narrowly defined jets show a clean and undisturbed structure, suggesting that such highly relativistic dynamics shields itself from rapid turbulence and destruction of the jet structure. (After a long propagation and emanation of its

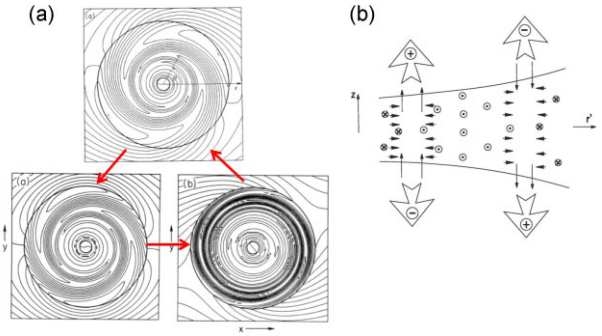

Figure 3. The physical consequences of the MRI. (A) Magnetic field is amplified by the winding motion due to the differential rotation of the accretion disc. When the field strength becomes too strong to be maintained by the accretion disc, it springs back to the less magnetized state, emitting a burst of Alfvénic disturbances (Gilden & Tajima 1985; Haswell et al. 1992). (B) MRI produces an electro-static field, which accelerates charged particles and heats up the disc halo. They eventually produce low-energy photons in keV–MeV energy range (Haswell et al. 1992).

energy, the jet begins to deplete, and then the jet motion starts to interact strongly with the surrounding intergalactic plasma, forming cocoon-like swollen clouds of plasma instabilities as seen at the end of each jet in Fig. 1). We consider intense wakefield formation in these jets, triggered by the episodic events of large bulk accretion driven by the MRI (Balbus & Hawley 1991) process in the accretion disc (Matsumoto & Tajima 1995), which can cause a large pulse of shear motion of the magnetic fields at the root of the plasma jet (Ebisuzaki & Tajima 2014a). We find from our estimate that the induced wakefields normalized intensity, $a_0 \equiv qE/m\omega c$, is as large as 10^{10} (ultrarelativistic regime of WFA; Tajima et al. 2020), which implies $v_{\rm tr} \approx c$. In general, the greater the relativistic intensity (i.e. a_0) is, the stronger are the coherence and integrity of the wakefields (Tajima 2010). Therefore, we expect that the resultant wakefields can persist over quite a large spatial extent within the jets. The Alfvén speed, $v_{\rm A}$, in a jet is nearly equal to the speed of light due to the generally very strong magnetic field and low plasma density. Since $v_{\rm tr} \sim v_{\rm ph} = v_{\rm A} > > v_{\rm th}$, the condition is met for stable acceleration of the bulk plasma in a jet.

Blandford & Znajek (1977) and Blandford & Payne (1982) are steady-state, ideal MHD theories and focus on local magnetic fields. An important implication from these theories is that jets are born magnetically dominated and therefore there must be a process or processes that convert this magnetic energy into kinetic energy. WFA may be one such process, and would also explain the long, coherent structure of jets given the increased stability at relativistic intensities (Tajima et al. 2020). Our theory assumes a constantly evolving, fluctuating, global magnetized accretion disc (see Fig. 3). The triggering of an Alfvénic burst that excites a wakefield is dependent upon global (entire disc) magnetic field instabilities. When a global magnetic field is present in a Keplerian rotating accretion disc, Balbus–Hawley type instabilities (MRI) are unavoidable. Matsumoto & Tajima (1995) showed the beta parameter can vary from 100 to < 1 in the accretion disc (also see equations 4.32 and 4.28 in Tajima & Shibata 1997) due to the MRI. Furthermore, jet formation requires a global field theory (Shibata & Uchida 1986; Balbus & Hawley 1991; Haswell, Tajima & Sakai 1992; Tajima & Shibata 1997). The strength of the magnetic field and the size of the perturbation, which depends on the BH mass, dictate the intensity of the Alfvén wave, similar to how the MR power scales with the mass of the BH (Kadowaki, Pino & Singh 2015; Singh, de Gouveia Dal Pino & Kadowaki 2015). The beta and magnetization parameters of the accretion disc may indirectly affect the intensity of the waves and how frequently they are launched, but fine tuning of model parameters can account for this and the physics remains the same, as will be shown.

The dynamics of ultrarelativistic WFA are distinct from MR. MR accelerates particles via the magnetic component of the Lorentz force in magnetic discontinuities. In WFA it is the pondermotive force of the electromagnetic wave that drives electrons ahead of the wave. The wake, a large depression in the plasma density behind the wave, traps positively charged particles that are accelerated by the electrostatic pull of the cluster of electrons ahead of them. MR and WFA would occur in different parts of the AGN–jet system. MR can occur in the accretion disc and in the jet before it becomes kinetically dominant (Medina-Torrejón et al. 2021). WFA occurs solely in the jet and the acceleration direction is always parallel to the wave vector. The wakefield travelling along the jet can remain coherent and accelerate particles virtually the entire length of the jet (Ebisuzaki & Tajima 2014a).

It should also be mentioned that MR plays an important role in disc–jet evolution in addition to particle acceleration. Gouveia Dal Pino & Lazarian (2005) and de Gouveia Dal Pino, Kowal & Lazarian (2013) showed that violent MR of the jet and disc fields accelerates and injects particles from the disc into the jet. Nishikawa et al. (2020) showed that at larger scales kinetic instabilities in the jet plumes can drive MR and is capable of accelerating electrons and protons. MR and MRI are intimately related, likely occurring together or sequentially. The accretion disc must fluctuate magnetically due to Keplerian twisting of the disc, stretching the field lines until the magnetic resistivity is great enough that matter accretes on to the BH. Once the field strength has reached its threshold, magnetic energy is released via MR and intense Alfvénic pulses (like a rubber band snapping back to its relaxed state), which subsequently heats the disc corona, launches particles into the jet and accelerates them. While MR (Gouveia Dal Pino & Kowal 2015; Nishikawa et al. 2020; Medina-Torrejón et al. 2021) and shocks (Matthews, Bell & Blundell 2020) are capable of accelerating particles to ultrahigh energies, we will argue in the following sections that WFA may be responsible for the generation of the majority, and most energetic UHECRs, given its ease at coherently accelerating ultrarelativistic charged particles over parsec to kilo-parsec scales depending only on the mass of the central accreting object in galactic and extragalactic sources possessing jets.

We applied WFA theory to six candidates from a broad range of central BH or NS mass. In the proceeding sections, we first derive the formulae used in our predictions, then each case study is presented in descending order of mass: blazar TXS 0506+056 in Section 3, radio galaxy Centaurus A in Section 4, Seyfert galaxy NGC 1068 in Section 5, starburst galaxies M82 and NGC 0253 in Section 6 and 7, and finally microquasar SS 433 in Section 8. We survey and scrutinize general commonalities as well as specific characteristics of their various signals, including cosmic rays and UHE gamma rays. Localized UHECRs or neutrinos have been observed in all cases, except SS 433. These six astrophysical objects have vastly different central masses from 10^9 down to only several solar masses. None the less, their polar jets exhibit common phenomena of intense acceleration, and fundamentally in a linear fashion with a pulsed operation given the episodic motion associated with the central object's accretion disc (Gilden & Tajima 1985; Balbus & Hawley 1991). Thus, the direction of arrival of UHECRs is localized as well as accompanied by gamma-ray emission (due to the electron acceleration) with a specific separation in the arrival time of the signals. This is explained in Section 2. Neutrino arrival may be

coincidental, but delayed in time as well. In other words, though the mass scales differ vastly, the underlying mechanisms are remarkably common; the burst periods and rise and fall times may differ among cases, but the mass dependence and qualitative features are curiously common. This is what we wish to investigate in detail for our six astrophysical objects. The emerging picture is a surprisingly unified, integrated physical mechanism of WFA. In Section 9, we summarize the comparison of our research of these potential UHECR sources with observational data.

Before we close this section, let us mention a separate, but important related issue of the recent simultaneous observation of the gravitational waves (GWs; Misner, Thorne & Wheeler 1973) and gamma-rays from the collision of two NSs (Abbott et al. 2017). When LIGO observed the GW arrival (Abbott et al. 2017), it was suggested (Takahashi, Tajima & Hillman 2000) that a collision of two NSs can yield not only the emission of violent phenomena such as GWs, but also gives rise to the formation of an accretion disc and its jets. It follows that an eruption at the base of the jets, such as a massive accretion, produces WFA of electrons (and thus gamma-rays), following the emission of a GW. Thus, we see that the gamma-ray emission is an important indicator of the underlying physical process of the electron acceleration (by WFA) and alerts us to the importance of the multimessenger astrophysics approach.

2 AGN JET WAKEFIELD ACCELERATION MODEL

The emerging new mechanism of WFA of Tajima & Dawson (1979) has quite a different theoretical construct in contrast to a stochastic acceleration mechanism. It is based principally on a single astrophysical object such as an AGN and its accretion disc and associated jets. An accretion disc instability, such as the MRI, can introduce the rapid increase of the present magnetic fields in the disc, which triggers episodic disruption of the accretion disc and subsequent disturbances at the feet of the jets (Gilden & Tajima 1985; Mizuta et al. 2018). See Fig. 3. This disturbance may be considered as the trigger of intense electromagnetic (originally Alfvénic shock) pulses in the jets. According to Tajima et al. (2020), we evaluate the basic physical parameters for the range of astrophysical objects using WFA theory.

In the WFA theory, developed by T. Ebisuzaki and T. Tajima (Ebisuzaki & Tajima 2014a, b; Tajima et al. 2020), input parameters are m and $\dot{m}$. The former, m, the BH mass, normalized by the solar mass ($\mathrm{M}_\odot = 2.0 \times 10^{33}$ g), can be estimated by observations such as stellar dynamics, quasi-periodic oscillation (QPO)/recurrence period, and Eddington limit. The latter is the accretion rate, $\dot{m}$, normalized by the critical accretion rate, $\dot{M}_\mathrm{c} = \frac{2\pi c R_0}{3\epsilon\kappa_\mathrm{T}}$. Here, κ_T is the Thomson scattering opacity and $\epsilon = 0.06$ is the radiation efficiency of the disc. The non-dimensional accretion rate $\dot{m}$ can be calculated using the radiation luminosity given as

$$L_\mathrm{rad} = \frac{4\pi c G \mathrm{M}_\odot}{\kappa_\mathrm{T}} \dot{m} m, \tag{1}$$

which is proportional to the product of $\dot{m}$ and m. Note that we have assumed a value of $p = 0.5$ for the power-law jet-spreading index in our formulation (see appendix A). This value can be adjusted on a per-source basis to obtain a more accurate model, but we chose to use the same value for all objects due to lack of accurate data on jet angles. The radiation luminosity L_rad can be estimated by emission lines from the nucleus for the case of AGNs (blazars, radio galaxies, and Seyfert galaxies) or by the X-ray luminosity for the case of less massive BHs ($<1000\mathrm{M}_\odot$: intermediate and stellar mass BHs). Since X-rays are believed to be emitted directly from the accretion disc by thermal mechanisms (not necessarily from the jets by non-thermal mechanisms) in the less massive BHs, their anisotropies are minimal compared with those of gamma-rays.

When m and $\dot{m}$, or equivalently L_rad are given, WFA theory predicts the rise time $2\pi/\omega$ of the burst, the episodic recurrence time $1/\nu$, and the acceleration time D_3/c, as follows:

$$2\pi/\omega = \frac{R_0}{6\epsilon c} \alpha^{1/2} \dot{m} m, \tag{2}$$

$$1/\nu = \frac{\sqrt{6} R_0}{c} \alpha^{-1/2} m, \tag{3}$$

$$D_3/c = \frac{1}{36} \left(\frac{e^2 R_0^4}{4\pi^3 c^5 m_\mathrm{e}^2 \epsilon^5 \kappa_\mathrm{T}} \right)^{1/3} \alpha^{5/6} \dot{m}^{5/3} m^{4/3}, \tag{4}$$

where $R_0 = 6G\mathrm{M}_\odot/c^2 = 9.0 \times 10^5$ cm is the radius of the innermost stable orbit of a one solar mass BH, c the light velocity, α the 'alpha' disc parameter (Shakura & Sunyaev 1973), and e and m_e are the electron charge and mass, respectively.

The protons are accelerated in the back side of the bow wake (see Fig. 5 B). The maximum proton energy (UHECRs) is given as

$$W_\mathrm{max} = \frac{1}{9} \left(\frac{e^4 c^2 R_0^2}{2 m_e \epsilon^4 \kappa_\mathrm{T}^2} \right)^{1/3} z \Gamma \alpha^{2/3} \dot{m}^{4/3} m^{2/3}, \tag{5}$$

where Γ is the bulk Lorentz factor of the jet (see Fig. 4). The luminosity of UHECR is calculated as

$$L_\mathrm{UHECR} = \frac{\zeta \sigma \alpha^{1/2}}{6\epsilon} L_\mathrm{rad}, \tag{6}$$

where σ is the energy efficiency of the charged-particle acceleration, including the conversion of Alfven wave into electromagnetic waves, and

$$\zeta = \frac{\ln(W_\mathrm{max}/W_0)}{\ln(W_\mathrm{max}/W_\mathrm{min})}. \tag{7}$$

Here, $W_0 = 0.57 \times 10^{20}$eV.

On the other hand, the electrons are accelerated in the front side of the bow wake (Fig. 5 B), simultaneously with protons behind. The accelerated electrons emit high energy gamma-rays with the energies ranging GeV–PeV due to the collision with the magnetic perturbations.

The luminosity of gamma-rays is given as

$$L_\gamma = \frac{\sigma \alpha^{1/2}}{6\epsilon} L_{rad}. \tag{8}$$

For the reader's convenience, we summarize the scaling laws represented by the equations above in Table 1.

The UHECR flux at Earth is calculated as

$$F_\mathrm{UHECR} = 6.7 \times 10^{-1} \left[\frac{\mathrm{UHECRs}}{100\ \mathrm{km^2 yr}} \right] \left(\frac{d}{3.6\mathrm{Mpc}} \right)^{-2} \left(\frac{L_{rad}}{10^{42}\mathrm{ergs}^{-1}} \right) \tag{9}$$

for the case of iostropic radiation with $\ln(W_\mathrm{max}/W_\mathrm{min}) = 30, \alpha = 0.1$, and $\sigma = 0.1$.

Ultra-high-energy protons, accelerated by the wakefield, may collide with another proton in the plume of decelerated material in the jet or interstellar gas near to produce pions, which decay into gamma rays, electrons, and neutrinos. The neutrino flux at Earth, F_ν, can be obtained from

$$W_\nu^2 F_\nu = \frac{f_{pp} \sigma \alpha^{1/2} L_{rad}}{6\Omega d^2 \epsilon \ln W_\mathrm{max}/W_{min}} \tag{10}$$

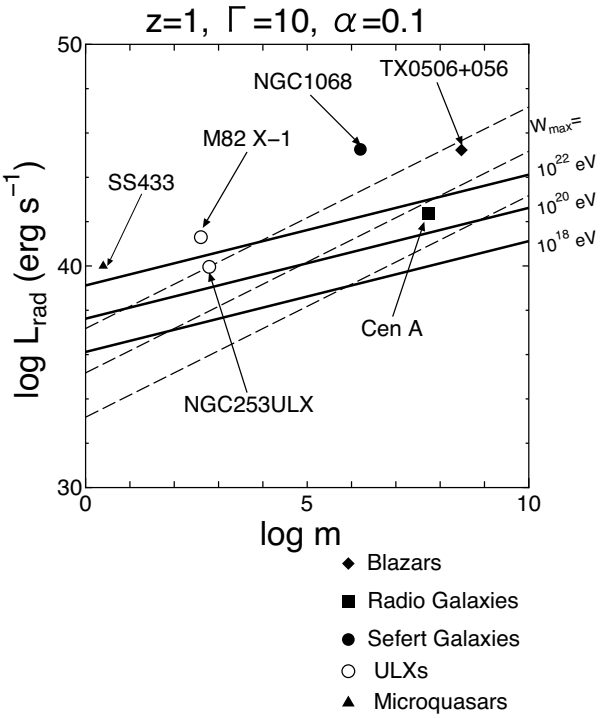

Figure 4. The maximum energies of protons, $W_{\rm max}$, are predicted using the mass of the central BH (normalized by one solar mass), m, on the right abscissa, and total radiation luminosity, $L_{\rm rad}$, by the WFA theory (Tajima et al. 2020) on the left abscissa. Various astronomical objects, such as microquasars (m = 1–10), ultraluminous X-ray sources (ULXs; m = 100–10 000) in starburst galaxies, central BHs of Seyfert galaxies $m \sim 10^6$ and radio galaxies/blazars ($m = 10^7$–10^{10}) can accelerate UHECRs with energy above 10^{20} eV. The individual points (or boxes) are plotted based on their known (or estimated) central mass according to our theory. Here, we assume the charge is $z = 1$, the bulk Lorentz factor of the flow of the jets $\Gamma = 10$, and $\alpha = 0.1$ the 'α' parameter of the disc. From top to bottom, the three dashed lines represent $\dot{m} = 10^{-1}$, 10^{-3}, and 10^{-5}.

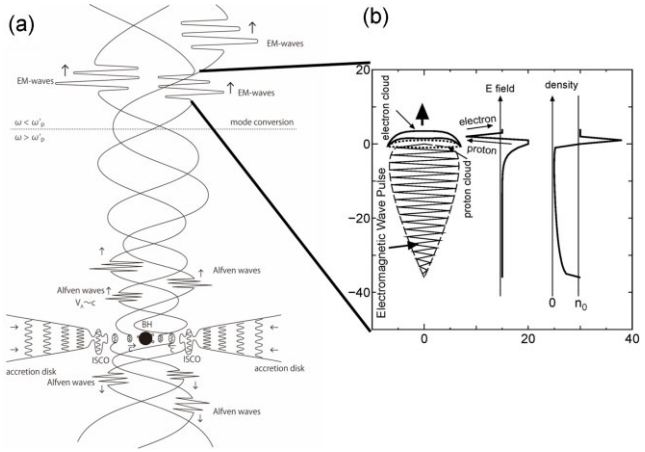

Figure 5. WFA theory for the accreting BH–jet system of an AGN (Ebisuzaki & Tajima 2014a, b; Tajima et al. 2020). (A) The cross-section of an AGN, its accretion disc and jets. Alfvén waves generated upon large mass accretions at the base of the jet propagate along the field line of the jet. They eventually mode-convert into intense electromagnetic waves when the wave frequency matches the local plasma frequency, $\omega_{\rm p}' = (4\pi n_{\rm jet} e^2/m_{\rm e}\gamma\Gamma^3)^{1/2}$, where γ is the Lorentz factor of a trapped particle, and Γ is the bulk Lorentz factor of the jet. (B) The structure of the bow wake. An electron cloud is formed at the front (top) of the wave pulse and a proton cloud follows. The resultant electric field accelerates protons in the back side and electrons in the front side of the bow wake. Since this acceleration structure moves at a velocity close to the speed of light, the charged particles with the same velocity (light velocity) in the field are accelerated for a long time and distance.

where f_{pp} is the collision probability of protons, Ω is the solid angle of the emission ($\Omega = 4\pi$ for the isotropic case), and we assume $W_\nu = 0.05 W_p$, where W_p is the same as $W_{\rm max}$.

It may be possible that the angle at which the jet spreads out from the central accretion object alters these parameter values. Such an assumption is not made in the present model nor in our results, however, we have included alternate formulas for an arbitrary value of p in Appendix A.

3 BLAZAR: TXS 0506+056

TXS 0506+056 in constellation Orion is a blazar with a redshift of 0.3365 ± 0.0010 (Paiano et al. 2018), which corresponds to about 1.75 Gpc from Earth. TXS 0506+056 was first catalogued as a radio source in 1983 (Lawrence et al. 1983), and then confirmed to be a blazar (Massaro et al. 2009). Gamma-rays emitted from TXS 0506+056 were detected by the EGRET and Fermi-LAT missions (Lamb & Macomb 1997; Halpern, Eracleous & Mattox 2003; Abdo et al. 2010). In addition, radio observations have shown apparent superluminal motion in the jet (Richards et al. 2011).

On 2017 September 22, the IceCube Neutrino Observatory detected high-energy neutrinos coming from a direction consistent with this flaring gamma-ray blazar TXS 0506+056 (IceCube Collaboration 2018a). The most probable energy for the observed neutrino is around 190 TeV with a 90 per cent confidence level, and lower limit of 183 TeV, depending only weakly on the assumed astrophysical energy spectrum. This suggests the existence of high-energy protons or nuclei with tens of PeV generated in the jet of the Blazar. The detection of high-energy neutrinos suggests charged particles are accelerated parallel to the jet axis.

During approximately 2 weeks of the neutrino observation, a peak flux of gamma-ray emission around 5.3×10^{-7} cm^{-2} s^{-1} is also reported by Fermi-LAT, with an energy range between 0.1 and 100 GeV (IceCube Collaboration 2018b). The associated isotropic luminosity during the period reaches as high as 1.2×10^{47} erg s^{-1} (IceCube Collaboration 2018a). Analysing the data prior to the event, a long-term isotropic gamma-ray luminosity between 0.1 and 100 GeV is derived with an averaged value of 0.28×10^{47} erg s^{-1} over 9.5 yr of Fermi-LAT observations of TXS 0506+056 (IceCube Collaboration 2018a). According to their study, the neutrino emission coincides with a peak in very high energy (VHE) gamma-ray flux and a local minimum of the spectral index (Fig. 1 of IceCube

Table 1. Time-scales, maximum energy, and luminosities estimated by Tajima et al. (2020).

Quantities	Scaling laws	Units	Equation numbers
$2\pi/\omega$	$8.2 \times 10^{-5}\alpha^{-1/2}\dot{m}m$	s	(2)
$1/\nu$	$7.3 \times 10^{-5}\alpha^{-1/2}m$	s	(3)
D_3/c	$1.7 \times 10^{2}\alpha^{5/6}\dot{m}^{5/3}m^{4/3}$	s	(4)
$W_{\rm max}$	$3.2 \times 10^{-31} z\Gamma\alpha^{2/3}m^{-2/3}L_{\rm rad}^{4/3}$	eV	(5)
$L_{\rm rad}$	$1.5 \times 10^{38}\dot{m}m$	erg s^{-1}	(1)
L_γ	$2.78\sigma\alpha^{1/2}L_{\rm rad}$	erg s^{-1}	(8)
$L_{\rm UHECR}$	$2.78\sigma\zeta\alpha^{1/2}L_{\rm rad}$	erg s^{-1}	(6)

Table 2. Comparison of observed parameters (shaded) and theoretical parameters (without shade). Theoretical and observational values for a range of astrophysical objects, including a blazar (BL), a radio galaxy (RG), a Seyfert galaxy (SyG), starburst galaxies (SBG), and a micro-quasar (MQ).

Parameter	TX 0506+056	Cen A	NGC1068	M82	NGC 0253	SS 433
type	BL	RG	SyG	SBG	SBG	MQ
$\log d$ (pc)	9.24	6.53	7.15	6.56	6.54	3.54
$\log M_{\rm BH}(M_\odot)$	8.48	7.74	6.20	2.60	2.79	0.40
$\log L_{\rm rad}(\rm erg\,s^{-1})$	45.23	42.36	45.26	41.30	39.96	40.00
$\log W_{\rm max}$ (eV)	24.49	21.16	26.05	23.17	21.26	22.91
$\log L_{\rm UHECR}$ ($\rm erg\,s^{-1}$)	43.17	40.31	43.20	39.24	37.90	37.94
$F_{\rm UHECR}(/100\,\rm km^2/yr)$	–	0.69	–	0.052	0.0026	–
$F_{\rm UHECR}(/100\,\rm km^2/yr)$	–	0.016	–	0.040	0.013	–
$\log 2\pi/\omega$ (s)	3.47	0.62	3.50	−0.46	−1.81	−1.76
$\log 2\pi/\omega$ (s)	<4.68	–	–	–	–	–
$\log 1/\nu$ (s)	4.84	4.10	2.56	−1.04	−0.85	−3.24
$\log 1/\nu$, (s)	<6.38	4.18	–	−0.70	<2.0	<1.0
$\log L_\gamma$ ($\rm erg\,s^{-1}$)	44.17	41.31	44.20	40.24	38.90	38.94
$\log L_\gamma$ ($\rm erg\,s^{-1}$)	47.08	38.04	45.53	40.18	39.78	37.57

Collaboration 2018b), which is similar to fluctuations of the spectral index caused by the MRI as depicted in Fig. 7 in Canac et al. (2020).

The coincidental detection of high-energy signals encouraged us to test WFA as an alternative explanation. According to the WFA theory, the relativistic pondermotive acceleration in the jet can boost particles to an energy over ZeV (Ebisuzaki & Tajima 2014a, b; Tajima et al. 2020). Also, because the particles are accelerated linearly, the corresponding signal detected can be highly beamed and emitted axially from the jets. In the rest of the section, we will estimate several physical parameters using our WFA model and compare them with their analogous observational value.

Mass estimation is difficult in general for blazars. Padovani et al. (2019), however, estimated the central BH mass to be $3 \times 10^8\,\rm M_\odot$ using the relations of BHs mass and R-band bulge magnitude $M(R) \sim -2.9$ (Paiano et al. 2017, 2018), assuming the host galaxy to be a giant elliptical. The bolometric luminosity ($\simeq L_{\rm rad}$) of $1.7 \times 10^{45}\,\rm erg\,s^{-1}$ takes into account the overestimation due to the jet-induced component of the bolometric luminosity derived from the O II and O III lines ($L_{\rm O\,II} = 9 \times 10^{45}\,\rm erg\,s^{-1}$ and $L_{\rm O\,III} = 3 \times 10^{45}\,\rm erg\,s^{-1}$), respectively. Substituting $m = 3 \times 10^8$ and $L_{\rm rad} = 1.7 \times 10^{45}\,\rm erg\,s^{-1}$ into equations (5), (2), and (3), we derived $W_{\rm max} = 3.1 \times 10^{24}$eV, $2\pi/\omega = 3.0 \times 10^3$ s, $1/\nu = 6.9 \times 10^4$ s, and $L_\gamma = 1.5 \times 10^{44}\,\rm erg\,s^{-1}$, as shown in Table 2.

Greisen (1966) and Zatsepin & Kuzmin (1966) (GZK) showed that UHE protons travelling through the cosmic microwave background will undergo inelastic collisions with photons, limiting the maximum energy of UHECRs that travelled 100 Mpc to 10^{20} eV. If this distance is shorter, however, the attenuation is less, and the opposite is true if the source is farther away. Given the distance between the source and Earth, the attenuated maximum energy can be calculated. This *attenuated* value for $W_{\rm max}$ can then be substituted into equation (7) to obtain a more accurate prediction of UHECR flux and luminosity that terrestrial observers might detect. We have not accounted for this effect in our calculations, because there are additional factors that can reduce the energy and flux of UHECRs and they are difficult to account for. We have already mentioned the jet-spreading index p and the anisotropy of UHE particles emitted from jets, but extragalactic magnetic fields and gaseous clouds also attenuate UHECR luminosity.

According to the MAGIC observation (Ansoldi et al. 2018) VHE gamma-rays, above 90 GeV, from TXS 0506+056 varied, increasing by a factor of 6 within a day. We may set $2\pi/\omega = 4.8 \times 10^4$ s or shorter as an e-raising time. There are two periods (2017 October 3–4, and October 31) of enhanced gamma-ray emission. We may set $1/\nu$ as 2.4×10^6 s or shorter, taking into account the incomplete observation in TeV gamma-rays.

The theoretical gamma-ray luminosity is calculated as $L_\gamma = 1.5 \times 10^{44}$ erg s^{-1} (see equation 8), which is much less than the observed isotropic gamma-ray luminosity $2.8 \times 10^{46}\,\rm erg\,s^{-1}$ observed by FERMI-LAT (IceCube Collaboration 2018a). This is likely due to the underestimation of the total luminosity as a result of the large distance (1.75 Gpc) between us and the blazar.

If the actual emission is strongly beamed, assuming isotropic emission will overestimate the luminosity by integrating the whole sphere. If we assume a 10° angle of spread for the beam, the corrected estimation of the Fermi-LAT luminosity will be 2 orders of magnitude lower than their reported value. That is, $L_\gamma^{(10^\circ)} = 4.6 \times 10^{44}\,\rm erg\,s^{-1}$, which is consistent with the theoretical luminosity.

Here, W_ν and $W_{\rm p}$ are the energies of the neutrino and the proton, respectively. Substituting $f_{\rm pp} = 1.0$, $L_{\rm rad} = 1.7 \times 10^{45}\,\rm erg\,s^{-1}$, d = 1.8 Gpc, $\sigma = 0.1$, $\alpha = 0.1$, $\epsilon = 0.06$, $\Omega/4\pi = 4.8 \times 10^{-2}$ for $\theta = 10^\circ$, and $\ln(W_{\rm max}/W_{\rm min}) = 30$ into equation (10), we obtain $F_\nu = 8.1 \times 10^{-16}\,\rm TeV^{-1}\,cm^{-2}\,s^{-1}$ at 100 TeV. It is consistent within 50 per cent of the observed flux by IceCube of $F_\nu = 1.6 \times 10^{-15}\,\rm TeV^{-1}\,cm^{-2}\,s^{-1}$ at 100 TeV (IceCube Collaboration 2018a).

WFA theory might explain the simultaneous arrival of high-energy gamma-rays and neutrinos from blazars, because particles are linearly accelerated and would continue travelling along the jet's axis once emitted. Our WFA model gives an underestimated gamma-ray luminosity compared to the observational data. This discrepancy may be explained by the localization of the beam-like emission in contrast to the isotropic emission. The periodicity of neutrino bursts may be qualitatively explained by fluctuations of the MRI that trigger intense electromagnetic pulses, which accelerates protons to become UHECRs and produces VHE gamma-rays. Although it can be difficult to detect the highest energy particles at present, future studies may find more evidence to support our theory.

4 RADIO GALAXY: CENTAURUS A

Centaurus A (also known as NGC 5128), in constellation Centaurus, is a radio galaxy with kpc size jets, and is 3.4 Mpc from the Earth

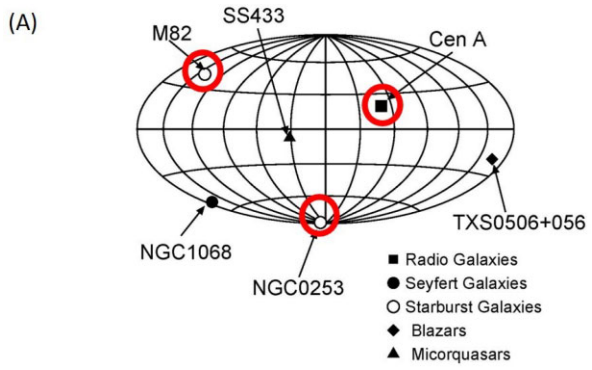

Figure 6. Prominent candidates of pin-pointed UHECR emission. Based on morphology of the candidates and their existing data, WFA theory predicts M82, NGC0253, Cen A, and NGC4945 are promising UHECR sources. The three hotspots in the observed skymap (red circles) of UHECRs $>6 \times 10^{19}$ eV (Aab et al. 2018) are consistent with prediction.

(Israel 1998). Cen A hosts an AGN believed to be a supermassive BH, whose mass is well defined by stellar dynamics (Neumayer 2010) to be $m = 5.5 \times 10^7$. The radiation luminosity is also determined to be $L_{\rm rad} = 2.3 \times 10^{42}$ erg s^{-1} from X-ray observations (Jourdain et al. 1993). Substituting the mass and radiation luminosity into equations (5), (2), (3), and (8) give us $W_{\rm max} = 1.4 \times 10^{21}$ eV, $2\pi/\omega = 4.2$ s, $1/\nu = 1.3 \times 10^4$ s, and $L_\gamma = 2.0 \times 10^{41}$ erg s^{-1}, as shown in Table 2.

Our theory predicts that Cen A is capable of accelerating protons to energies above 10^{21} eV (see Table 2). If we assume isotropic emission of UHECRs, their predicted flux is 0.60 /km^2 /yr. However, Aab et al. (2018) observed UHECRs as energetic as 10^{20} eV arriving from the direction of Cen A (Fig. 6) with an observed flux of 0.016 /km^2 /yr. As mentioned in the previous section, the large discrepancy in the perceived UHECR flux is likely due to the fact that the jets of Cen A are oriented nearly perpendicular to our line-of-sight (LOS), thus the vast majority of cosmic rays, especially the most energetic, ejected from its jets never reach Earth. Intergalactic magnetic fields may deflect some less-energetic protons towards Earth to become UHECRs. The episodic recurrence time predicted by our model is consistent with the observation of Fukazawa et al. (2011) and Rothschild et al. (2011), who detected fluctuating X-ray luminosity in the time-scale of 10–20 ks ($1/\nu \sim 1.5 \times 10^4$) (see Table 2).

Cen A has been known to emit gamma-rays in the range of TeV and greater for decades now. The H.E.S.S. telescope measured a gamma-ray flux of $0.45 \pm 0.07 \times 10^{-13}$ ph cm^{-2} s^{-1}TeV^{-1} at 1 TeV (Fig. 4 in Aharonian et al. 2009) with a corresponding total gamma-ray luminosity of 1.1×10^{38} erg s^{-1} (H. E. S. S. Collaboration 2018). The factor of ∼2000 difference between the theoretical and observational value for L_γ is again likely due to the fact that the axis of the jets are at a large angle to our LOS, and naturally gamma-ray emissions are strongly beamed in the axially direction of the jets in the context of WFA.

5 SEYFERT GALAXY NGC 1068

NGC1068 is a Seyfert galaxy that has a bright nucleus with a central BH of 1.6×10^6 M$_\odot$ (Goulding et al. 2010). It is also undergoing an intense starburst process. It is located at a distance of 14 Mpc (Tully & Fisher 1988) in the constellation Cetus. A bolometric luminosity of the nucleus of 1.8×10^{45} erg s^{-1} was obtained from O IV line (Goulding et al. 2010). Substituting $m = 1.6 \times 10^6$, $L_{\rm rad} = 1.8 \times 10^{45}$ erg s^{-1}, and $\alpha = 0.1$ into equations (5), (2), (3), and (8) gives us $W_{\rm max} = 1.1 \times 10^{26}$ eV, $2\pi/\omega = 3.2 \times 10^3$ s, $1/\nu = 3.63 \times 10^2$ s, $L_\gamma = 1.6 \times 10^{44}$ erg s^{-1} (see Table 2).

Since $W_{\rm max} > 10^{20}$ eV, NGC 1068 is capable of efficiently accelerating charged particles to UHE levels. In fact, isotropic UHECR is as high as ∼ 30 UHECRs/100 km^2 /yr (Table 2), though the spot size would be too large (70 degree or more) due to intergalactic magnetic fields and a distance to Earth three times larger than M82, Cen A, and NGC 0253 (Globus, Allard & Parizot 2008).

There is no significant luminosity change in the intrinsic luminosity from the accretion disc of the nucleus of NGC 1068. Although Zaino et al. (2020) reported a time variability on the scale of 1–6 months, the detailed spectral analysis revealed that the variability is not due to the change in the intrinsic accretion rate but due to the change in the obscuring Compton thick cloud ($N_{\rm H} > 10^{25}$ cm^{-2}) (Matt et al. 2004), which surrounds the nucleus. This view is consistent with the IR and optical observations (Taranova & Shenavrin 2006; Hönig & Kishimoto 2011).

Ackermann et al. (2012) observed isotropic gamma-ray luminosity of 1.5×10^{41} erg s^{-1}. This is inconsistent with the model prediction above (see Table 2). On the other hand, Acciari et al. (2019) more recent results set an upper limit of gamma-ray flux above 200 GeV at 5.1×10^{-13} erg cm^{-2} s^{-1}. It corresponds to an isotropic luminosity of 3.5×10^{45} erg s^{-1}, which is slightly more than one order of magnitude larger when compared with the theoretical prediction.

The IceCube collaboration reported the positive detection of neutrinos at 1 TeV of 3×10^{-13} TeV^{-1} cm^{-2} s^{-1} from NGC 1068 (Aartsen et al. 2020). Substituting $m = 1.6 \times 10^6$, $L_{\rm rad} = 1.8 \times 10^{45}$ erg s^{-1}, $\Omega = 4\pi$, and $\alpha = 0.1$ into equation (10), we obtain the theoretical isotropic flux as 2.2×10^{-11} TeV^{-1} cm^{-2} s^{-1}. In other words, WFA theory can explain IceCube observation, if 1 per cent of the neutrinos emitted from the jets travel towards Earth; the neutrinos from the jets are most likely to be strongly beamed.

It is possible there are two primary sources of neutrinos emitted from an AGN: MR in the accretion disc, and WFA in the jets. Khiali & de Gouveia Dal Pino (2016) showed that MR in the disc can account for neutrino emission below 10 PeV in BL Lacs and low-luminosity AGNs. Rodriguez-Ramirez et al. (2019) did the same for Cen A, the nearest AGN whose jets happen to be nearly perpendicular to our LOS providing good resolution of the Galactic Centre. WFA is capable of creating neutrinos well beyond 10 PeV by accelerating protons to ZeV energies and beyond, which then collide with slower protons. Our estimate for the neutrino flux at 100 TeV for blazar TXS 0506+056 is within 50 per cent, but our estimate for NGC 1068, whose jets are not aligned with our LOS, at 1 TeV was roughly 2 orders of magnitude larger. Therefore, it may be the case that WFA can only explain axially emitted neutrinos, produced in the jet, far away from the central object. Future observations of neutrino emissions from blazars could confirm this.

6 STARBURST GALAXY: M82

M82 is a starburst galaxy at a distance of 3.6 Mpc from Earth (Freedman et al. 1994) in the constellation Ursa Major. The starburst activity takes place in a relatively small central region, radius of ∼200 pc (Völk, Aharonian & Breitschwerdt 1996) from the dynamic centre of the galaxy.

Ultraluminous X-ray (ULX) sources of luminosity $\gtrsim 10^{40}$ erg s^{-1} inside M82 has been observed (see Xu, Liu & Liu 2015 and the

references therein). Among them, M82 X-1 is the brightest ULX in M82, located about 200 pc away from the dynamic centre of the galaxy (Matsumoto & Tsuru 1999; Tsuru et al. 2004; Dewangan, Titarchuk & Griffiths 2006; Patruno et al. 2006; Feng & Kaaret 2010). There has been a lot of discussions in the past 20 yr regarding the mass of M82 X-1, which has converged to the intermediate mass range, in other words 10^2–10^3 $M_\odot$. We adopt the mass of 400 $M_\odot$ by Pasham, Strohmayer & Mushotzky (2014), who used QPO frequency to fit a mass value. Substituting $m = 4 \times 10^2$ and $L_{\rm rad} = 2 \times 10^{41}$ erg s^{-1}, and $\alpha = 0.1$ into equations (5), (2), (3), and (8), we computed $W_{\rm max} = 1.5 \times 10^{23}$ eV, $2\pi/\omega = 3.5 \times 10^{-1}$ s, $1/\nu = 9.1 \times 10^{-2}$ s, and $L_\gamma = 1.7 \times 10^{40}$ erg s^{-1}, as shown in Table 2.

The WFA theory predicts that M82 X-1 is capable of accelerating protons and nuclei to energies above 10^{20}eV, in spite of its less massive BH ($\sim 400\,M_\odot$; Table 2). In fact, the Telescope Array (TA) team suggested that there is a hotspot in the northern sky of arrival direction of the UHECRs above 57 EeV (Abbasi et al. 2014; see also Fig. 6) in close proximity to M82.

He et al. (2016) divided the events belonging to the northern hotspot into two by energy, and found that there was a systematic deviation between them. Assuming that this is due to the deflection by the magnetic field (Globus et al. 2008), the position of the true source was estimated. While the estimated position, though extended to 10 degrees, included several high-energy celestial objects such as M82 and Mrk 180, only M82 was located within the GZK-horizon (100 Mpc) that the UHECRs could reach. The TA team detected 72 cosmic rays of 57 EeV in 5 yr. Among them, 19 events are within the hotspot (Abbasi et al. 2014), while 4.5 events were expected from uniform arrival. Since the effective area of TA is 700 km^2, the observed excess flux in the hotspot direction is about 0.040 UHECRs/100 km^2/yr, which is in good agreement with the expected isotropic flux from equation (6) (~ 0.052 UHECRs/100 km^2/yr, as shown in Table 2).

The QPO period of M82 X-1 is observed in X-ray band to be 0.2 s (Pasham et al. 2014). As we have carried out in Sections 3 and 5, the theoretical recurrence time is $1/\nu = 9.23 \times 10^{-2}$ s (Table 2). This predicted value is consistent with the QPO period within a factor of two.

In the WFA theory, electrons can also be accelerated in a similar way that protons are (see Fig. 5 B). This is separate from the electron cloud that is accelerated in front of the electromagnetic wave. The high-energy electrons, accelerated in the wakefield in the direction of the jet, emit gamma rays by synchrotron radiation due to interaction with magnetic perturbations in the jets. As previously mentioned the gamma-ray luminosity of M82 X-1 is predicted to be 1.7×10^{40} erg s^{-1} (Table 2). On the other hand, a bright and isolated gamma-ray excess, consistent with the location of the position of M82 of 100 MeV to 700 GeV gamma-rays that are isotropic in luminosity of 1.5×10^{40} erg s^{-1} with FERMI-LAT (Ackermann et al. 2012). This is consistent with the theoretical prediction, though it might just be chance, taking into account the anisotropic nature of WFA theory (particle trajectories are predominantly linear). We cannot observe M82 and its jets along their axis (like a blazar), therefore observational data samples oblique emissions, which we have used in our model predictions. Although it is encouraging that our predictions are consistent with data, both heavily underreport the true total luminosity, and flux of each signal.

7 STARBURST GALAXY: NGC 0253

NGC 0253 is a nearly edge-on starburst galaxy located 3.5 ± 0.2 Mpc from the Earth (Rekola et al. 2005) in the constellation Sculptor. Aab et al. (2018) reanalysed the data of arrival direction observed by Pierre Auger Observatory (PAO) and found that a significant (4σ level) enhancement in the arrival direction map of UHECRs above 39 EeV with the search radius of 12.9 degree towards nearby starburst galaxies, NGC 0253 (Fig. 6). The result is consistent with the data of TA team, though statistically marginal (Aab et al. 2018; Attallah & Bouchachi 2018).

Gutiérrez, Romero & Vieyro (2020) proposed two candidates for the source of UHECRs, one is TH2 (Turner & Ho 1985) and the other is NGC253 X-1. Although TH2 was presumed the brightest radio source nearly coincident to the centre of the galaxy, the recent observation by ALMA revealed that the position of TH2 exactly coincides to one of the knots in the central region of NGC 0253, which are most likely H II regions excited by young compact star clusters. The mass of the clusters is estimated as 10^6 $M_\odot$ and is not likely to have any BHs, since there are no X-ray emissions. Although one may still assume a hidden non-accreting BH in the cluster, any BH without accretion cannot emit any energy. Gutiérrez et al. (2020) assumed a strong magnetic field of 10^4 G around the BH to produce jet luminosity through the Blandford–Znajek effect (Blandford & Znajek 1977). However, this magnetic field will decay rapidly if there is no matter accreting on the BH, and thus the luminosity in equation (3) of Gutiérrez et al. (2020) is not sustainable. In conclusion, TH2 is unlikely to be a source of UHECRs.

ULX sources, on the other hand, are promising as UHECR sources, such as NGC 0253 X-1, if we take into account WFA. NGC 0253 harbours at least three ULXs with the luminosity ranging between (2.4 and 4.1) $\times 10^{39}$ erg s^{-1} (Barnard 2010). The sum of the luminosities of the ULXs reaches 9.1×10^{39} erg s^{-1} as shown in Table 2. They are considered to be intermediate BHs with masses that range from 10^2 to 10^4 $M_\odot$. In fact, we can estimate the mass to be 6.1×10^2 $M_\odot$ by substituting $\alpha = 0.1$, $L_{\rm rad} = 9.1 \times 10^{39}$ erg s^{-1}, and $\dot{m} = 0.1$ into equation (1). Substituting $m = 6.1 \times 10^2$ and $L_{\rm rad} = 9.1 \times 10^{39}$ erg s^{-1}, and $\alpha = 0.1$ into equations (5), (2), (3), and (8), we can derive $W_{\rm max} = 1.8 \times 10^{21}$ eV, $2\pi/\omega = 1.5 \times 10^{-2}$ s, $1/\nu = 1.4 \times 10^{-1}$ s, and $L_\gamma = 7.9 \times 10^{38}$ erg s^{-1}, as shown in Table 2.

The maximum energy of protons is estimated to be $W_{\rm max} = 1.8 \times 10^{21}$ eV. The expected UHECR flux (0.013 UHECRs/100 km^2/yr) is approximately a factor of 5 larger than the observed flux (0.0026 UHECRs/100 km^2/yr) for the isotropic distribution, as seen in Table 2 within of a factor of five.

The episodic recurrence time is estimated by our WFA model to be $1/\nu = 1.4 \times 10^{-1}$ s. Barnard (2010) reports significant variabilities can be seen in 100 s bin, which are much longer when compared with the theoretical predictions. Since observations for very short time variabilities (less than seconds) have unfortunately not been done for the ULXSs in NGC 253, the theory is not constrained by the observations.

The theoretical gamma-ray luminosity is estimated to be $L_\gamma = 7.9 \times 10^{38}$ erg s^{-1}. The observed gamma-ray luminosity (isotropic) is 6.0×10^{39} erg s^{-1} in 1–100 GeV (Ackermann et al. 2012), which is one order of magnitude higher than the expected gamma-ray flux. Direct comparison of L_γ luminosity with our model is difficult, however, due to other contributions from supernova remnants (Eichmann & Tjus 2016).

8 MICROQUASAR: SS 433

SS 433 is a galactic binary system consisting of a supergiant star $M = 10$–30 $M_\odot$ and a compact object of $M = 2$–3 $M_\odot$ (commonly considered to be a BH) in the constellation Aquarius. The distance to

the SS 433 system was estimated to be 3.5 kpc (Blundell & Bowler 2004) and is located inside of the supernova remnant W50, which exploded 17–24 thousands years ago (Goodall, Alouani-Bibi & Blundell 2011). SS433 jet's have an approximate length of 40 pc, and a bulk velocity of 0.26c (Margon et al. 1984; Fabrika 2004). The two precessing jets model is well established (Abell & Margon 1979; Fabian & Rees 1979; Milgrom 1979; Hjellming & Johnston 1981; Katz et al. 1982).

Kubota et al. (2010) determined the mass of the compact object from orbital analyses to be 2.5 $M_\odot$. According to Cherepashchuk et al. (2005) and Abeysekara et al. (2018), the jet luminosity is as high as 10^{40} erg s^{-1}, because of supercritical accretion, in spite of very low luminosity (10^{35-36} erg s^{-1}) in the X-ray band (Safi-Harb & Ögelman 1997). Substituting $m = 2.5$, $L_{\rm rad} = 1.0 \times 10^{40}$ erg s^{-1}, and $\alpha = 0.1$ into equations (5), (2), (3), and (8), we derived $W_{\rm max} = 8.1 \times 10^{22}$ eV, $2\pi/\omega = 1.7 \times 10^{-2}$ s, $1/\nu = 5.8 \times 10^{-4}$ s, and $L_\gamma = 8.7 \times 10^{38}$ ergs^{-1}, as shown in Table 2.

According to our WFA model, SS433 is capable of accelerating protons, and thus a potential source for UHECRs; in fact, the maximum acceleration energy $W_{\rm max}$ is as high as 3.5×10^{21} eV (Table 2). The UHECRs produced in SS433, may not be very localized unfortunately, since it is located near the Galactic Centre, where the magnetic field is large compared with the outer region. It may produce a broad (more than several 10 degrees) concentration towards the Galactic Centre, together with other microquasars in the Galactic Centre region (Tajima et al. 2020).

Although a significant variation in flux at the time-scale of 10 s was observed (Revnivtsev et al. 2006), there is no information in the millisecond range. Therefore, our prediction for the recurrence time, $1/\nu = 5.8 \times 10^{-4}$, is unconstrained by observation.

The model-predicted gamma-ray luminosity is $L_\gamma = 8.7 \times 10^{38}$ erg s^{-1} (Table 2). Since gamma-rays are strongly beamed in the direction of the jets, they are not necessarily seen from Earth; our LOS is not aligned with the jets of SS433. The angle between our LOS and the axis of the jet precession is about 74 degrees (Davydov, Esipov & Cherepashchuk 2008) and the precession angle is about 20 degrees (Cherepashchuk et al. 2005). Careful analysis of data from the Fermi gamma-ray observatory Large Area Telescope reveals that the SS433 system emits gamma-rays with a peak around 250 MeV. It showed a modulation of $\sim 10^{-10}$ erg cm^{-2} s^{-1} correlation with the precession period (Rasul et al. 2019). The corresponding isotropic luminosity is 3.6×10^{37} erg s^{-1}. This component may be related to the gamma-rays emitted from the electrons accelerated by wakefield in the jets, as suggested by Tajima et al. (2020), though the observed flux is much less compared with the theoretical prediction for the case of isotropic emission, again likely due to the oblique angle between our LOS and the jet axis.

At 20 TeV, the HAWC detector reported the emission is spatially localized in the three lobes (e1, e2, and w1), 40 pc away from the SS433 system (Abeysekara et al. 2018). Since the lobes are located where the jets interact with the nebula gas, the gamma-rays are expected to be primarily a result of synchrotron emission from high-energy electrons accelerated by the bow-shock which then collide with a magnetic field of ~ 10 μGauss produced by the interaction of jets with nebula clouds.

Galactic BH binaries, such as SS433, Cyg X-1, Cyg X-3, and Sco X-1, exhibit relativistic jets, violent variabilities in time-scales ranging from milliseconds to years, and emit radiation from radio to VHE gamma-rays ($\sim$ TeV). Because of such non-thermal phenomena, they are considered counterparts of quasars ($\sim 10^{6-9}$ $M_\odot$) in million times smaller scales with masses of ~ 10 $M_\odot$ (i.e. micorquasars) yet they are capable of generating high-energy gamma-rays and UHECRs.

9 CONCLUSIONS

The objects that we have detailed above, in reality, are only a few 'good candidates' out of tens and maybe even hundreds or thousands of blazars, quasars, and microquasars that possess jets of parsec to kiloparsec length and are capable of accelerating charged particles to energies $>10^{19}$ eV. WFA is almost certainly present in all astrophysical objects that have 'jets,' regardless if they are as small as a binary star (10–100 Ms) or as large as blazars ($\geq 10^8$ Ms); the parameter values change, but the physics is the same (or similar). Although we have primarily focused on extragalactic jets as candidates for WFA – resulting in pinpointed emission of UHECRs and correlated, localized emission of gamma rays with pronounced structure – through Sections 3–7, we also find that jets from much smaller objects, namely microquasars in our own Galaxy, are also capable of emitting UHECRs (including neutrinos) and simultaneously gamma-rays (see Section 8). In fact our theory anticipates that much more microquasars are potential sources of a variety of signals including UHECRs.

Tables 2 summarizes the measurables of the six astrophysical objects we surveyed in relation to their observed properties along with the theoretically derived values. More accurate predictions of the UHECR flux and luminosity can be calculated if the GZK limited maximum energy is substituted for $W_{\rm max}$ in equation (7). However, this is a straightforward calculation, and so we chose in favour of reporting the unattenuated values to illustrate the capability of WFA at generating UHE charged particles in astrophysical jets of all sizes. In Section 2, we adopted reasonable values for several model parameters including, but not limited to, $p, \kappa_T, \epsilon, \alpha$ since it is beyond the scope of this paper to determine accurate values for each and every model parameter on a per source basis. We expect that the model predictions would be closer to their observational counterparts if more accurate values were used in the calculations. Despite some inaccuracy in the model parameters, WFA theory implies that the flux of all emitted particles and photons will be greatest when the observers LOS is parallel to the jet axis, such as the case for blazars. This is because wakefields travel parallel to the jet and thus trapped charged particles accelerated by the wake also travel, and are eventually emitted parallel to the jet assuming little or no deflection from extrinsic factors. It is reasonable then to assume that the flux of these signals has a radial dependence on the distance from the jet axis that decreases outward. This may explain why we have only observed neutrinos from blazars, and not quasars. Furthermore, the most energetic particles are more likely to be emitted parallel or very near parallel to the jet axis since they are least susceptible to being perturbed. The anisotropy in emission of course also implies that the amount of observable UHECRs, gamma rays, etcetera produced by nearby quasars and microquasars is less than it otherwise would be if their jets were oriented (anti)parallel to our LOS. Thus, it is expected that our model predictions would over estimate observational data.

Our theory and predictions suggest that WFA is very capable of generating cosmic rays with energies equal to and even greater than the most energetic UHECRs that have ever been detected, as well as UHE gamma-rays and neutrinos. Many quasars and microquasars alike show evidence of being pinpointed origins of UHE gamma-rays and UHECRs (and sometimes neutrinos) including the six objects studied herein. We acknowledge, however, that shock acceleration

and MR are also potential sources for lower energy signals such as cosmic rays below 10^{18} eV (before synchrotron radiation becomes insurmountable at large gamma factors), and most of the synchrotron emissions of VHE gamma-rays down to radio frequencies. In particular, MR may be capable of generating UHECRs as well.

A linear acceleration mechanism, such as WFA, is not hindered by deleterious synchrotron emissions. Furthermore, in the special case of blazars, our theory can explain time signatures, specifically anticorrelations in the spectral index and flux (Fig. 7 in Canac et al. 2020) observed in blazar 3C 453.4 that steady-state theories, such as Fermi acceleration, cannot. Neutrino bursts, coincidental with gamma-ray bursts originating from blazars have recently been detected (Garrappa et al. 2019; Rodrigues et al. 2021). This is also readily explained by WFA since it accelerates a large pocket of electrons ahead of the wave that emit gamma-rays due to their orbit or collisions with magnetic inhomogenities, and pockets of UHE protons behind that can undergo collisions with slower protons to produce neutrinos, thereby creating simultaneous 'bursts' of UHECRs, neutrinos, and gamma-rays. For decades astronomers have known that knots within AGN jets propagate very near the speed of light, for example Cen A (Israel 1998; Snios et al. 2019). This may be understood from WFA that it is natural to have extremely energetic, periodic structures that occur in the jets, part of which contain bow wakes (Ebisuzaki & Tajima 2014a, b; Tajima et al. 2020) that form dense pockets of electrons propagating ahead of the pulse, and protons behind it.

WFA sheds new light on interesting time evolving processes, such as fluctuations in the spectra of blazars, and the movement, and acceleration of matter inside astrophysical jets, and now even neutrino bursts. WFA coupled with the MRI may be able to provide a virtually complete picture of the generation of UHECRs, UHE gamma rays, and dynamical time signature bursts and fluctuations from start to finish; beginning with MRI causing disc eruption and massive accretion of matter, and ending with the extremely fast particles colliding with decelerated particles in gaseous lobes at the end of the jets (to produce secondary particles and gamma-rays), or in Earth's atmosphere as UHECRs.

We previously stated in Section 1 that the condition for stable, bulk plasma acceleration via wakefields is satisfied since $v_{\rm tr} \sim v_{\rm ph} > > v_{\rm th}$. This does not imply that the entire plasma in the vicinty of the wakefield is trapped and accelerated for the duration of the wave. Instead, slower particles are accelerated for a lesser amount of time and even slower particles will experience multiple kicks as they randomly pass through accelerating-decelerating phases of the wake when the wave contains multiple frequencies. Chen, Tajima & Takahashi (2002) showed that the stochasticty of the kicks generates a power-law dependence of the particle energy spectrum with an index equal to 2. Lau et al. (2015) simulated relativistic WFA using a 1D PIC code and plotted the resulting energy spectrum of the plasma in their Fig. 7. We note that the spectral index from WFA (Mima et al. 1991; Chen et al. 2002) is similar to that of shock acceleration, however, the index can become greater than 2 in the case of WFA, see for example Fig. 4 in Canac et al. (2020). This is important for explaining the anticorrelations in flux and spectral-index of blazars.

We should also note that lower energy phenomena of these objects such as localized emissions of radio waves, soft X-rays with high intensities may be attributable to the disturbances arising not from the jets, but from the accretion disc itself. This may be a result of the MRI (not as well-organized as WFA in the jets) that arises from the accretion disc itself. This is briefly explained in Fig. 3. See Haswell et al. (1992), Okuda et al. (1992), Mineshige (1993), Smith, Haswell & Hynes (2006), and Liu, Gu & Zhang (2017). The time correlations (or lack of them) in this lower energy range of emissions, along with high-energy gamma-rays and UHECRs (or neutrinos) may provide the subtle relation between the halo dynamics, exterior and interior discs, and jets. In Appendix A, we explore a variation introduced by the spread of the jet, which changes theoretical values in Table 2.

The magnetic energy stored in an accretion disc obeys a power-law dependence on the BH mass (Shakura & Sunyaev 1973). This energy is the source from which both disc–jet MR and MRI (Balbus & Hawley 1991; Ebisuzaki & Tajima 2014a) draw their power from. That is why Fig. 2 in Singh et al. (2015), and multiple figures in Kadowaki et al. (2015) show plots very similar to Fig. 4.

We strongly encourage further verification of WFA theory in our Universe be conducted via multimessenger observations including TeV gamma-ray telescope facilities, such as the Cerenkov Telescope Array (CTA; Actis et al. 2011), GW detectors like Advanced LIGO (Aasi et al. 2015), the VIRGO (Accadia et al. 2011), and KAGRA (Akutsu et al. 2018), and ultra-high-energy cosmic rays/neutrino observatories, such as Probe of Extreme Multi-Messenger Astrophysics, (POEMMA; Anchordoqui et al. 2020), and The Giant Radio Array for Neutrino Detection (GRAND; Alvarez-Muniz et al. 2020). We hope WFA theory and the work presented here can contribute to these observational efforts.

ACKNOWLEDGEMENTS

We would like to thank Professors S. Bird, S. Barwick, K. Abazajian, H. Sobel, J. Bullock, G. Mourou, X.Q. Yan, T. Tait, S. Murgia, P. Picozza, P. Klimov, S. Bulanov, T. Esirkepov, K. Nakajima, the late Y. Takahashi, the late J. A. Wheeler, and the JEM-EUSO collaboration for their kind discussions that helped carry out this work. This work started as a term project report by students who participated in the University of California, Irvine graduate course Physics 249 'Plasma Astrophysics' (Spring, 2020), in which the instructor (TT) guided the subject of wakefields in astrophysics. This work was supported by the Rostoker Fund (TT) as well as an APS (American Physical Society) GPAP (Topical Group in Plasma Astrophysics) student travel grant (GBH) for the 2021 APS DPP (Division of Plasma Physics) meeting.

DATA AVAILABILITY

The data underlying this article are available in the article and the references herein.

REFERENCES

Aab A. et al., 2018, ApJ, 853, L29
Aartsen M. G. et al., 2020, Phys. Rev. Lett., 124, 051103
Aasi J. et al., 2015, Class. Quantum Gravity, 32, 074001
Abbasi R. U. et al., 2014, ApJ, 790, L21
Abbott B. P. et al., 2017, ApJL, 848, 59
Abdo A. A. et al., 2010a, ApJ, 709, L152
Abdo A. A. et al., 2010b, ApJ, 715, 429
Abell G. O., Margon B., 1979, Nature, 279, 701
Abeysekara A. U. et al., 2018, Nature, 562, 82
Abraham J. et al., 2008, Astropart. Phys., 29, 188
Accadia T. et al., 2011, Class. Quantum Gravity, 28
Acciari V. A. et al., 2019, ApJ, 883, 135
Ackermann M. et al., 2011, ApJ, 743, 171 ,
Ackermann M. et al., 2012, ApJ, 755, 164
Actis M. et al., 2011, Exp. Astron., 32, 193
Aharonian F. et al., 2009, ApJ, 695, L40

Akutsu T. et al., 2018, Prog. Theor. Exp. Phys., 2018, 013F01
Alvarez-Muniz J. et al., 2020, Sci. China Phys. Mech. Astron., 63, 219501
Anchordoqui L. A. et al., 2020, Phys. Rev. D, 101, 083532
Ansoldi S. et al., 2018, ApJ, 863, L10
Asada K., Nakamura M., 2012, ApJ, 745, L28
Attallah R., Bouchachi D., 2018, MNRAS, 478, 800
Balbus S., Hawley J., 1991, ApJ, 376, 214
Barnard R., 2010, MNRAS, 404, 42
Bell A. R., 1978, MNRAS, 182, 147
Blandford R., Eichler D., 1987, Phys. Rep., 154, 1
Blandford R. D., Payne D. G., 1982, MNRAS, 199, 883
Blandford R. D., Znajek R. L., 1977, MNRAS, 179, 433
Blundell K. M., Bowler M. G., 2004, ApJ, 616, L159
Canac N. E., Abazajian K. N., Tajima T., Ebisuzaki T., Horiuchi S., 2020, MNRAS, 493, 2229
Chatterjee K., Liska M., Tchekhovskoy A., Markoff S. B., 2019, MNRAS, 490, 2200
Chen P., Tajima T., Takahashi Y., 2002, Phys. Rev. Lett., 89, 161101
Cherepashchuk A. M. et al., 2005, A&A, 437, 561
Davydov V. V., Esipov V. F., Cherepashchuk A. M., 2008, Astron. Rep., 52, 487
de Gouveia Dal Pino E. M., Kowal G., 2015, in Lazarian A., de Gouveia Dal P., Elisabete M., Melioli C., eds, Magnetic Fields in Diffuse Media. Springer, Berlin Heidelberg, p. 373
de Gouveia Dal Pino E. M., Lazarian A., 2005, A&A, 441, 845
de Gouveia Dal Pino E. M., Kowal G., Lazarian A., 2013, in Pogorelov N. V., Audit E., Zank G. P., eds, ASP Conf. Ser. Vol. 488, Fermi Acceleration in Magnetic Reconnection Sites. Astron. Soc. Pac., San Francisco, p. 8
Dewangan G. C., Titarchuk L., Griffiths R. E., 2006, ApJ, 637, L21
DeYoung T., 2012, Nucl. Instrum. Methods Phys. Res. A, 692, 72
di Matteo A., Fujii T., Kawata K., 2019, EPJ Web Conf., 210, 01007
Djannati-Atai A., 2009, Nucl. Instrum. Methods Phys. Res. A, 602, 28
Ebisuzaki T., Tajima T., 2014a, Astropart. Phys., 56, 9
Ebisuzaki T., Tajima T., 2014b, Eur. Phys. J. Spec. Top., 223, 1113
Eichmann B., Tjus J. B., 2016, ApJ, 821, 87
Fabian A. C., Rees M. J., 1979, MNRAS, 187, 13P
Fabrika S., 2004, Astrophys. Space Phys. Res., 12, 1
Feng H., Kaaret P., 2010, ApJ, 712, L169
Freedman W. L. et al., 1994, ApJ, 427, 628
Fukazawa Y. et al., 2011, ApJ, 743, 124
Garrappa S. et al., 2019, ApJ, 880, 103
Gilden D., Tajima T., 1985, Proc. IAU Symp. 107, Unstable Current Systems and Plasma Instabilities in Astrophysics. Kluwer, Dordrecht, p. 477
Globus N., Allard D., Parizot E., 2008, A&A, 479, 97
Goodall P. T., Alouani-Bibi F., Blundell K. M., 2011, MNRAS, 414, 2838
Goulding A. D., Alexander D. M., Lehmer B. D., Mullaney J. R., 2010, MNRAS, 406, 597
Greisen K., 1966, Phys. Rev. Lett., 16, 748
Gutiérrez E. M., Romero G. E., Vieyro F. L., 2020, MNRAS, 494, 2109
H. E. S. S. Collaboration, 2018, A&A, 619, A71
Halpern J. P., Eracleous M., Mattox J. R., 2003, AJ, 125, 572
Haswell C., Tajima T., Sakai J.-I., 1992, ApJ, 401, 495
He H.-N., Kusenko A., Nagataki S., Zhang B.-B., Yang R.-Z., Fan Y.-Z., 2016, Phys. Rev. D, 93, 043011
Hjellming R. M., Johnston K. J., 1981, ApJ, 246, L141
Hönig S. F., Kishimoto M., 2011, A&A, 534, A121
IceCube Collaboration, 2018a, Science, 361, 147
IceCube Collaboration, 2018b, Science, 361, eaat1378
Israel F. P., 1998, A&AR, 8, 237
Jackson J. D., 1999, Classical Electrodynamics. Wiley, New York
Jourdain E. et al., 1993, ApJ, 412, 586
Kadowaki L. H. S., Pino E. M. d. G. D., Singh C. B., 2015, ApJ, 802, 113
Katz J. I., Anderson S. F., Margon B., Grandi S. A., 1982, ApJ, 260, 780
Khiali B., de Gouveia Dal Pino E. M., 2016, MNRAS, 455, 838
Kole M., 2021, CERN Cour., 61, 11
Kotera K., Olinto A. V., 2011, ARA&A, 49, 119
Kubota K. et al., 2010, PASJ, 62, 323
Lamb R. C., Macomb D. J., 1997, ApJ, 488, 872
Lau C., Yeh P., Luk O., McClenaghan J., Ebisuzaki T., Tajima T., 2015, Phys. Rev. Spec. Top., 18, 024401
Lawrence C. R., Bennett C. L., Garcia-Barreto J. A., Greenfield P. E., Burke B. F., 1983, ApJS, 51, 67
Liu T., Gu W.-M., Zhang B., 2017, New Astron. Rev., 79, 1
Margon B., Anderson S. F., Aller L. H., Downes R. A., Keyes C. D., 1984, ApJ, 281, 313
Massaro E., Giommi P., Leto C., Marchegiani P., Maselli A., Perri M., Piranomonte S., Sclavi S., 2009, A&A, 495, 691
Matsumoto R., Tajima T., 1995, ApJ, 445, 767
Matsumoto H., Tsuru T. G., 1999, PASJ, 51, 321
Matt G., Bianchi S., Guainazzi M., Molendi S., 2004, A&A, 414, 155
Matthews J. H., Bell A. R., Blundell K. M., 2020, New Astron. Rev., 89, 101543
Medina-Torrejón T. E., de Gouveia Dal Pino E. M., Kadowaki L. H. S., Kowal G., Singh C. B., Mizuno Y., 2021, ApJ, 908, 193
Michelson P. F., Atwood W. B., Ritz S., 2010, Rep. Prog. Phys., 73, 074901
Milgrom M., 1979, A&A, 76, L3
Mima K., Horton W., Tajima T., Hasegawa A., 1991, AIP Conf. Proc. Vol. 230, Nonlinear Dynamics and Particle Acceleration. Am. Inst. Phys., New York, p. 27
Mineshige S., 1993, Astrophys. Space Sci., 210, 83
Misner C., Thorne K., Wheeler J., 1973, Gravitation. W H Freeman and Co, San Francisco
Mizuta A., Ebisuzaki T., Tajima T., Nagataki S., 2018, MNRAS, 479, 2534
Neumayer N., 2010, Publ. Astron. Soc. Aust, 27, 449
Nishikawa K. et al., 2020, MNRAS, 493, 2652
O'Neil T., 1965, Phys. Fluids, 8, 2255
O'Sullivan S., Reville B., Taylor A. M., 2009, MNRAS, 400, 248
Okuda T., Ono K., Tabata M., Mineshige S., 1992, MNRAS, 254, 427
Padovani P., Oikonomou F., Petropoulou M., Giommi P., Resconi E., 2019, MNRAS, 484, L104
Paiano S., Landoni M., Falomo R., Treves A., Scarpa R., 2017, ApJ, 844, 120
Paiano S., Falomo R., Treves A., Scarpa R., 2018, ApJ, 854, L32
Pasham D. R., Strohmayer T. E., Mushotzky R. F., 2014, Nature, 513, 74
Patruno A., Portegies Zwart S., Dewi J., Hopman C., 2006, MNRAS, 370, L6
Pushkarev A. B., Kovalev Y. Y., Lister M. L., Savolainen T., 2017, MNRAS, 468, 4992
Ragan K., 2012, Nucl. Instrum. Methods Phys. Res. A, 692, 24
Rasul K., Chadwick P. M., Graham J. A., Brown A. M., 2019, MNRAS, 485, 2970
Rekola R., Richer M., McCall M., Valtonen M., Kotilainen J., Flynn C., 2005, MNRAS, 361, 330
Revnivtsev M. et al., 2006, A&A, 447, 545
Richards J. L. et al., 2011, ApJS, 194, 29
Rodrigues X., Garrappa S., Gao S., Paliya V. S., Franckowiak A., Winter W., 2021, ApJ, 912, 54
Rodriguez-Ramirez J. C., de Gouveia Dal Pino E. M., Alves Batista R., 2019, in Proceedings of International Conference on Black Holes as Cosmic Batteries: UHECRs and Multimessenger Astronomy—PoS(BHCB2018). SISSA Medialab, p. 014
Rothschild R. E., Markowitz A., Rivers E., Suchy S., Pottschmidt K., Kadler M., Mueller C., Wilms J., 2011, ApJ, 733, 23
Safi-Harb S., Ögelman H., 1997, ApJ, 483, 868
Shakura N. I., Sunyaev R. A., 1973, A&A, 24, 337
Shibata K., Uchida Y., 1986, Astrophys. Space Sci., 118, 443
Singh C. B., de Gouveia Dal Pino E. M., Kadowaki L. H. S., 2015, ApJ, 799, L20
Smith A., Haswell C., Hynes R., 2006, MNRAS, 369, 1537
Snios B. et al., 2019, ApJ, 871, 248
Tajima T., 2010, Proc. Japan Acad. B, 86, 147
Tajima T., Dawson J. M., 1979, Phys. Rev. Lett., 43, 267
Tajima T., Shibata K., 1997, Plasma Astrophysics. Addison-Wesley, Reading, Mass
Tajima T., Yan X. Q., Ebisuzaki T., 2020, Rev. Mod. Plasma Phys., 4, 7

Takahashi Y., Tajima T., Hillman L., 2000, in Tajima T., Mima K., Baldis H., eds, Relativistic Lasers and High Energy Astrophysics. Kluwer, Springer US, p. 171
Taranova O. G., Shenavrin V. I., 2006, Astron. Lett., 32, 439
Tsuru T. G., Matsumoto H., Inui T., Matsushita S., Kawabe R., Harashima T., Maihara T., Iwamuro F., 2004, Prog. Theor. Phys. Suppl., 155, 59
Tully R. B., Fisher J. R., 1988, Nearby Galaxies Catalogue. Cambridge Univ. Press, Cambridge
Turner J. L., Ho P. T. P., 1985, ApJ, 299, L77
Völk H. J., Aharonian F. A., Breitschwerdt D., 1996, Space Sci. Rev., 75, 279
Xu X.-jie, Liu J., Liu J., 2015, ApJ, 799, L28
Zaino A. et al., 2020, MNRAS, 492, 3872
Zatsepin G., Kuzmin V., 1966, J. Exp. Theor. Phys. Lett., 4, 78

APPENDIX A: DEPENDENCE OF WAKEFIELD ON THE JET SPREAD

As we have examined in previous Sections 3–8, in interpreting the individual astrophysical objects and phenomena only one model may serve as sufficient in understanding those astrophysical objects. While the general theory we described through the excitation of the disc disturbances, including shaking of the jets, and the subsequent wakefield generation and acceleration of particles along the jets have turned out to be quite generic and deep rooted physics common among these objects and their phenomena, despite its disparate scales and mass differences of the central objects. There are some important individualities that may matter in detailed manifestations of the objects and parameters. One example of such may be the jet's spreading angle. Jets may be strongly collimated by the spiraling surrounding magnetic fields. This may relax certain constraints on phenomena and parameters. Here we introduce the jet spreading by one model parameter of the power index that determines the jet diameter as a function of the distance from the central object, as the jet particles and magnetic fields emanate outward.

We discuss the dependence of physical parameters in the jet on distance from the bottom and how the waves propagate through it. First, we assume that

$$b(D) = R_0 m((D/R_0 m)^p + 1) \tag{A1}$$

where $b(D)$ is the radius of the jet at distance D from the bottom of the jet. Although the power-law index, p, is observed to be close to ∼0.5 for the case of M87, the closest active galactic nuclei (Asada & Nakamura 2012), and many other AGN jets (Pushkarev et al. 2017), it may fall in the range of 0 (a cylinder) to 1 (a linear cone) for other AGNs and microquasars.

The cyclotron frequency ω_c' in the jet corrected for relativistic effects is given by

$$\omega_{\rm c}' = \frac{eB_{\rm jet}}{m_{\rm e}c\gamma} \tag{A2}$$

On the other hand, the magnetic field $B_{\rm jet}$ in the jet can be calculated assuming that the magnetic field flux is conserved in the jet.

$$B_{\rm jet} = [B_{\rm disk}(r=1)](b/mR_0)^{-2} \tag{A3}$$

$$= [B_{\rm disk}(r=1)]\left(\frac{D}{mR_0}\right)^{-2p} + 1 \tag{A4}$$

$$= \left(\frac{16\pi c^2}{3\sqrt{6}\kappa_{\rm T} R_0}\right)^{1/2} m^{-1/2}\left(\frac{D}{mR_0}\right)^{-2p} \tag{A5}$$

Next, we assume

$$\gamma = a_0 \tag{A6}$$

within the jet. a_0 can be calculated, assuming that the wave intensity in the jet is conserved, i.e. the flux $\phi_{\rm w,\,jet}$ is inversely proportional to the cross-sectional area πb^2 of the jet.

$$a_0(D) = a_0(D = R_0)\left(\frac{b(D)}{R_0 m}\right)^{-1} \tag{A7}$$

where D is the distance from the bottom of the jet, and $b(D)$ is the radius of the jet, which is assumed to be $b(0) = 3R_g = R_0 m$. In addition, Fig. 5 shows the ratio ω_c'/ω of the cyclotron frequency to the wave frequency and that of plasma frequency ω_p'/ω, plotted against the distance $D/(R_0 m)$ from the bottom of the jet for the typical cases ($\Gamma = 10$, $\alpha = 0.1$, $\xi = 10^{-2}$, $\dot{m} = 0.1$, and $m = 1$, 10^4, 10^8). Here now, we get

$$a_0(D) = \frac{\rm e}{36 m_{\rm e} c}\sqrt{\frac{R_0}{\pi\epsilon^3\kappa_{\rm T}}}\alpha^{3/4}\dot{m}^{3/2}m^{1/2}\left(\frac{D}{R_0 m}\right)^{-p} \tag{A8}$$

Substituting equations (A5) and (A6) into equation (A2), we obtain

$$\omega_{\rm c}' = \frac{144c\pi}{R_0}\left(\frac{\epsilon^3}{3\sqrt{6}}\right)^{1/2}\frac{1}{\alpha^{3/4}\dot{m}^{3/2}m}\left(\frac{D}{R_0 m}\right)^{-2p} \tag{A9}$$

On the other hand, the plasma frequency $\omega_{\rm p}'$ corrected for relativistic effects is given by

$$\omega_{\rm p}' = \left(\frac{4\pi n_{\rm jet} e^2}{m_{\rm e}\gamma\Gamma^3}\right)^{1/2} \tag{A10}$$

The plasma density $n_{\rm jet}$ in the jet can be solved for as follows, if we assume the kinetic luminosity of the jet:

$$L_{\rm jet} = n_{\rm jet}\mu m_{\rm H} c^3 \Gamma^2 \pi b^2 = \xi L_{\rm rad} \tag{A11}$$

is conserved through the jet.

$$n_{\rm jet} = \frac{2}{3\mu m_{\rm H}\kappa_{\rm T} R_0}\frac{\xi\dot{m}}{\Gamma^2 m}\left(\frac{D}{R_0 m}\right)^{(p-1)/2} \tag{A12}$$

Here, ξ is the ratio of the kinetic luminosity of the jet to the radiation luminosity, Γ is the bulk Lorentz factor, and $\mu = 1.29$ is the mean molecular weight of the accreting gas. Substituting equations (A8) and (A12) into equation (A10), we get

$$\omega_{\rm p}' = \left(\frac{4\pi n_{\rm jet} e^2}{m_{\rm e}\gamma\Gamma^3}\right)^{1/2} \tag{A13}$$

$$= \left(\frac{96\pi ec}{\mu m_{\rm H}}\right)^{1/2}\left(\frac{\pi\epsilon^3}{R_0\kappa_{\rm T}}\right)^{1/4}\frac{\xi^{1/2}}{\Gamma^{5/2}\alpha^{3/8}\dot{m}^{1/4}m^{3/4}}\left(\frac{D}{R_0 m}\right)^{(p-1)/2} \tag{A14}$$

For most of the interesting cases, the relationship of $\omega_{\rm c}'$, $\omega_{\rm p}' > \omega$ holds; In other words, at the bottom of the jets, the plasma in the over dense state ($\omega_{\rm p}' > \omega$), where plasma waves and electromagnetic waves cannot propagate. On the other hand, Alfvénic waves can propagate, since $\omega_{\rm c}' > \omega$. The Alfvén velocity $V_{\rm A,\,jet}$ at the bottom of the jet is given by

$$V_{\rm A,jet} = \frac{B_{\rm jet}}{\sqrt{4\pi m_{\rm H} n_{\rm jet}}} = \left(\frac{2}{\sqrt{6}}\right)^{1/2} c\frac{\Gamma}{\xi^{1/2}\dot{m}^{1/2}} \tag{A15}$$

In other words, the nominal values of the Alfvén velocity

$$V_{\rm A,jet} \sim 10^{12}[{\rm cm\,s^{-1}}]\left(\frac{\Gamma}{10}\right)\left(\frac{\xi}{10^{-2}}\right)^{-1/2} \tag{A16}$$

This can approach the speed of light, when the approximation breaks down. Then the wave becomes that of EM waves in magnetized plasma. On the other hand, $\omega_{\rm p}' = \omega$ at the distance D_2 given

by

$$\left(\frac{D_2}{R_0 m}\right) = \left[\frac{4R_0 e^2}{9\pi\mu^2 m_{\rm H}^2 c^2 \epsilon}\frac{\xi^2 \alpha^{1/2}\dot{m}^3 m}{\Gamma^{10}}\right]^{2(1-p)} \tag{A17}$$

Past the location of D_2 ($D > D_2$), $\omega > \omega'_{\rm p}$ so that the plasma wave (electromagnetic wave) is allowed to propagate. The electromagnetic waves propagated as Alfvén and whistler waves are converted into plasma waves (electromagnetic waves) by non-linear mode-conversion when the wave frequency matches the plasma frequency. This $D > D_2$ leads to the bow WFA as described in the next subsection.

The pondermotive force, $F_{\rm pm}$, which acts on the electrons caught in an intense electromagnetic wave is a force generated from the Lorentz force, $\left(\frac{v}{c}\right) \times B$, in the propagation direction of the electromagnetic wave. If the motion of the electrons by the wave is not relativistic ($a < 1$), it can be calculated as the force resulting from the average of the profiles of the electromagnetic pulses. In the relativistic regime ($a > 1$), this force is more simplified. Since the particle velocity asymptotically approaches the light velocity and if the plasma satisfies the under dense ($\omega > \omega'_p$) condition as well, then $B = E$. In this case, $F_{\rm pm}$, is given by

$$F_{\rm pm} = \Gamma m_{\rm e} e c a \omega \tag{A18}$$

Charged particles are accelerated by an electric field generated by bow wakefield (longitudinal polarization of electronic distributions). As shown in Fig. 5, protons are accelerated at the back slope of the wakefield, while electrons are accelerated at the front slope. The acceleration force $F_{\rm acc}$ is given by

$$F_{\rm acc} = zF_{\rm pm} = z\Gamma e E_{\rm w}\left(\frac{D}{R_0}\right)^{-p} \tag{A19}$$

$$= \frac{ec}{3}\left(\frac{\pi}{\epsilon\kappa_{\rm T} R_0}\right)^{1/2}\frac{z\Gamma\alpha^{1/4}\dot{m}^{1/2}}{m^{1/2}}\left(\frac{D}{R_0 m}\right)^{-p} \tag{A20}$$

Here, z is the charge of the particle. The maximum energy, $W_{\rm max}$, obtained by the particle is determined by integrating $F_{\rm acc}$ over the acceleration distance, D_3

$$W_{\rm max} = \int_0^{D_3} F_{\rm acc} dD \tag{A21}$$

$$= \frac{ec}{3}\left(\frac{\pi}{\epsilon\kappa_{\rm T} R_0}\right)^{1/2} z\Gamma\alpha^{1/4}\dot{m}^{1/2} m^{1/2}\int_0^{D_3}\left(\frac{D}{R_0 m}\right)^{-p} dD \tag{A22}$$

$$= \frac{2ec}{3}\left(\frac{\pi R_0}{\epsilon\kappa_{\rm T}}\right)^{1/2} z\Gamma\alpha^{1/4}\dot{m}^{1/2} m^{1/2}\left(\frac{D_3}{R_0 m}\right)^{1-p} \tag{A23}$$

The acceleration distance, D_3, is evaluated as

$$D_3 = \frac{e}{432 m_{\rm e} c}\left(\frac{R_0^3}{\pi^3\epsilon^5\kappa_{\rm T}}\right)^{1/2}\alpha^{5/4}\dot{m}^{5/2} m^{3/2}\left(\frac{D_3}{R_0 m}\right)^{-p} \tag{A24}$$

We can solve equation (A24) for $(D_3/R_0 m)$

$$\left(\frac{D_3}{R_0 m}\right) = \left(\frac{e}{432 m_{\rm e} c}\right)^{1/(1+p)}\left(\frac{R_0}{\pi^3\epsilon^5\kappa_{\rm T}}\right)^{1/2(1+p)} * \alpha^{5/4(1+p)}\dot{m}^{5/2(1+p)} m^{1/2(1+p)} \tag{A25}$$

Substituting equation (A25) into equation (A21), we obtain

$$W_{\rm max} = \frac{1}{3^{(4-2p)/(1+p)}}\left(\frac{\pi^{-2+4p} e^4 c^{4p} R_0^2}{2^{2-2p} m_{\rm e}^{2(1-p)}\epsilon^{6-4p}\kappa_{\rm T}^2}\right)^{1/2(1+p)} * z\Gamma\alpha^{(6-4p)/4(1+p)}\dot{m}^{(6-4p)/2(1+p)} m^{1/(1+p)} \tag{A26}$$

Here we can eliminate $\dot{m}$ as

$$W_{\rm max} = \frac{1}{6}\left(\frac{3^{2p} e^4 \kappa_{\rm T}^{4-4p}}{4\pi^{8-8p} m_{\rm e} c^{18-16p} R_0^{4-4p}\epsilon^{6-4p}}\right)^{1/2(1+p)} * z\Gamma\alpha^{(6-4p)/4(1+p)} m^{-2(1-p)/(1+p)} L_{rad}^{(6-4p)/2(1+p)} \tag{A27}$$

The p-dependent formulae in this section can be naturally reduced, if we take $p = 1/2$, in the 'standard case' for example, as was done in Section 2. It may be useful to incorporate such a dependence on the jet spreading (p-index) in assessing maximum proton energy from SS433, as well as other astrophysical objects.

This paper has been typeset from a TEX/LATEX file prepared by the author.